Simulation and Testbed Studies Aimed at Detecting Earth-Like Planets with NASA's Next-Generation Space-based SIM-Lite Astrometric Observatory

Benjamin Draper, Richard Jelsma, Dr. Ahktar Mahmood-Bellarmine University and Dr. Bijan Nemati-Jet Propulsion Laboratory

ABSTRACT

NASA is embarking on a bold mission to detect extra-solar Earth-like planets. By 2015 NASA will launch its most sophisticated next generation space-based SIM-Lite (Space Interferometry Mission) Observatory to search for Earth-like terrestrial planets in the habitable zone orbiting the nearby stars, located within 33 light-years. SIM-Lite will be the first space-based long baseline Michelson interferometer designed for precision astrometry with one micro-arcsecond (one billionth of a degree) accuracy. Finding Earth-like rocky planets is extremely challenging since Earth-like planets are small by comparison and are relatively close to their bright stars. An Earth-sized planet will be so close to the much brighter star that they are almost impossible to tell apart. Optical interferometry using new astrometric techniques can be used to detect Earth-like planets. An Earth-like planet will typically reveal their presence by small effects they have on their star. SIM-Lite instrument's ultra-precise resolution and sensitivity will detect the tiny wobble of a distant star being tugged by an orbiting extra-solar planet to within 20 pico-meters (a distance that is about 10 times smaller than an atom). We are currently working on the SCDU (Spectral Calibration Development Unit) testbed at JPL to determine how well we can make these ultra precise astrometric measurements. Using MATLAB, we have been working on a new wavefront reconstruction technique using the Misell algorithm to determine the instrument's optical performance. We will present the current results of our study. This research work is being funded by NASA's KSGC (Kentucky Space Grant Consortium) program.

INTRODUCTION AND METHODOLOGY

The SIM-Lite satellite (Figure 4) uses interferometry to measure movements of stars to a precision of one microarcsecond. Light from an observed star is diffracted by lenses and mirrors in the satellite to obtain the interference patterns necessary for this precision. Fourier transform methods are the principle tool to evaluate diffraction and interference of light waves. We have learned about and developed our ability to evaluate wavefronts of light using the mathematical and computer based techniques of Fourier analysis.

A HeNe laser with parallel, monochromatic light waves and having little divergence of its wavelets (which consist of many photons with the same phase and direction in a very small plane wave) is diffracted by a parabolic mirror onto a CCD camera which reproduces its image in 4 micron pixels on a computer screen. This experimental setup is used as a model which ultimately can be used as a tool to study the optics of SIM-Lite. Mathematically, the wavefront of the laser is modeled as a constant amplitude, radially symmetric, circular wavefront. Diffraction by the parabolic mirror produces an interference pattern in the focal plane of the lens. Aberrations in the mirror, or in a lens in the beam's path, will distort this ideal beam and its diffraction pattern and produce irregularities which are detected in the experimental images and which can be evaluated mathematically.
When a light wave is diffracted by a small aperture (or a parabolic mirror or lens), the amplitude of a point [U(x, y)] in the diffraction plane is defined by the Fraunhofer diffraction equation (which is a Fourier transform describing diffraction in far space), and these points can be assembled by a computer into a map of amplitude across all points in a diffraction plane. The Fraunhofer diffraction equation is

$$U(x,y) = \frac{e^{ikz} e^{\frac{ik}{2}(x^2+y^2)}}{i\lambda z} \iint_{\Sigma} U(\xi,\eta) e^{\frac{-i2\pi}{\lambda z}(x\xi+y\eta)} d\xi d\eta$$

where (x and y) are in the diffraction plane, (ξ and η) are in the aperture plane, (z) is a normal line between the planes, is an aperture function of the amplitude of a light wave's electrical field, and (λ) is the wavelength of the monochromatic laser.

$e^{\frac{-i2\pi}{\lambda z}(x\xi+y\eta)}$ is the elementary Fourier function which defines the frequency and direction of "frequency space"; because frequency and direction are defined in this way, the # of radians between points across the aperture (ξ,η) and the point being evaluated in diffraction space (x,y) can be precisely calculated. The terms outside the integral are constants and account for phase delays in the diffraction plane due to the normal divergence of photons in a wavefront. If diffraction is evaluated between confocal spherical mirrors, separated by exactly the right distance, $e^{\frac{ik}{2}(x^2+y^2)}$ the term disappears; this term accounts for the Huygens-Fresnel secondary wavelets which diverge parabolically, but not spherically as they predicted. [U(x, y)] is the value of this transform at a single point in the diffraction plane. For symmetric circular apertures, a Fourier transform can be simplified by using polar coordinates. If a circular aperture is symmetric, g(*r*, θ) = g(*r*) and the Fourier transform of an aperture can be described as $G(\rho,\phi) = G(\rho) = 2\pi \int_z g(r) J_0(2\pi r\rho) dr$ in which J_0 is a Bessel function of zero order, (ρ) is the radius for the circle of interest in the diffraction plane which is defined in terms of spatial frequency, (*r*) is the radius for the variable circle undergoing integration across the aperture, g(*r*) is the aperture function, G(ρ) is the Fourier transform for a single circle in the diffraction plane. $J_0(2\pi r\rho)$ is the elementary function which defines the frequency of diffraction space in the same way that $\left[e^{\frac{i2\pi}{\lambda z}(x\xi+y\eta)}\right]$ does this for rectangular coordinates. This function is called the Fourier-Bessel transform which is abbreviated as β[g(*r*)]. The *circ*(*r*) function defines a uniform, monochromatic wavefront with unit amplitude passing through a circular aperture. $\beta[circ(r)] = \frac{J_1(2\pi\rho)}{\rho}$ in which J_1 is a Bessel function of the first order. The numerical values for the zero and first order Bessel functions are available in handbooks and so a polar Fourier transform greatly simplifies a transform's solution. Applying β[*circ*(*r*)] to the Fraunhofer integral requires several mathematical adjustments but the result for the intensity of the light pattern in the diffraction plane is simply $I(r) = \left(\frac{A}{\lambda z}\right)^2 \left[\frac{2J_1\left(\frac{kwr}{z}\right)}{\frac{kwr}{z}}\right]$ in which (*r*) now is the circular radius in the diffraction plane, (*w*) is the radius of the aperture, $A = \pi w^2$ is the area of the aperture, (λ) is the wavelength of the monochromatic light, (z) is the distance of a normal line between the aperture and diffraction planes, (*k*) is the wave number which equals (2π/λ). All of these terms, including J_1 are numbers most of which have units, and all are readily available. The photo on the Rt. is an Airy pattern of Fraunhofer diffraction from a circular aperture.

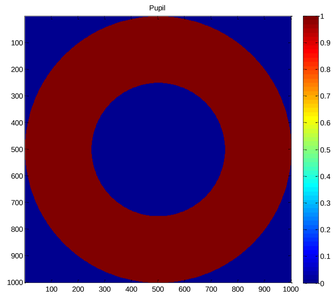

Figure 1. A Circular Pupil was created with a center aperture. This simulated the collimated beam seen in the test bed

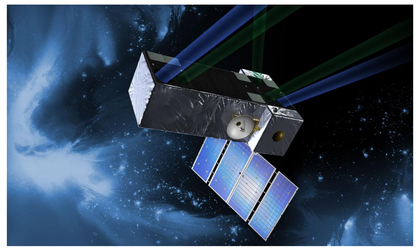

Figure 4. Artistic representation of the SIM-Lite Astrometric Observatory in space.

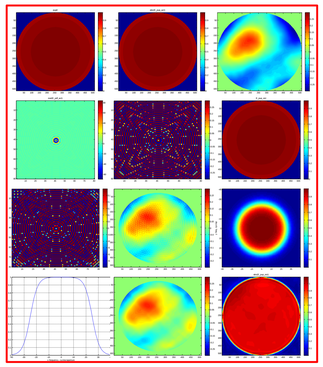

Figure 8. Refinement of initial Misell algorithm. Propagation from image plane with a broad filter.

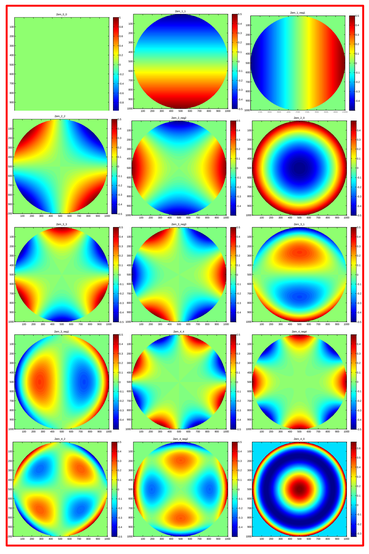

Figure 2. Using the Pupil created in Figure 1 Zernike Polynomials from 0 to 4 were displayed on the pupil at all corresponding frequencies. Zernike polynomials are important functions as they help to describe optical wavefront error.

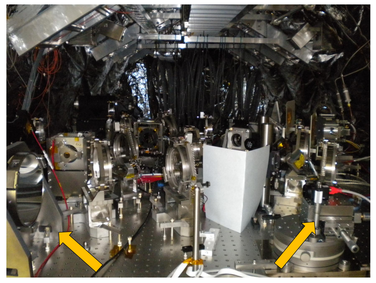

Figure 5. Optical bench inside the SCDU testbed shown with parabolic mirror (right) and data acquisition camera (left).

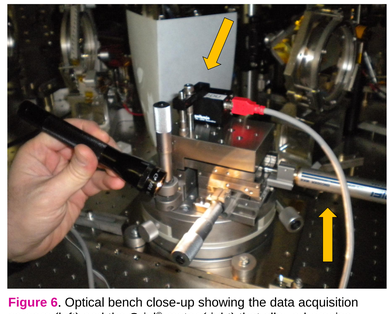

Figure 6. Optical bench close-up showing the data acquisition camera (left) and the Oriel® motor (right) that allowed precise position measurements.

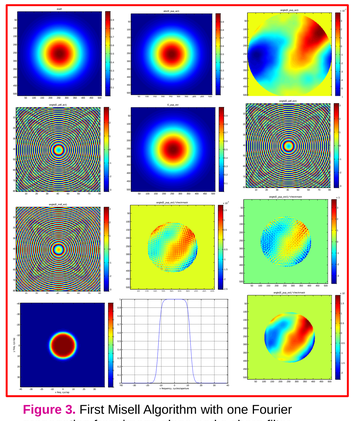

Figure 3. First Misell Algorithm with one Fourier propagation from image plane and a sharp filter

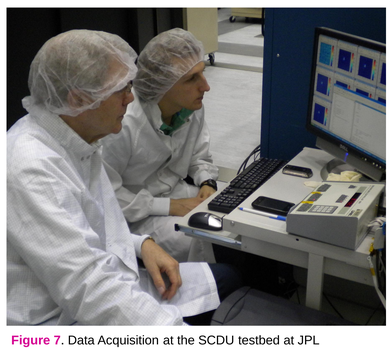

Figure 7. Data Acquisition at the SCDU testbed at JPL

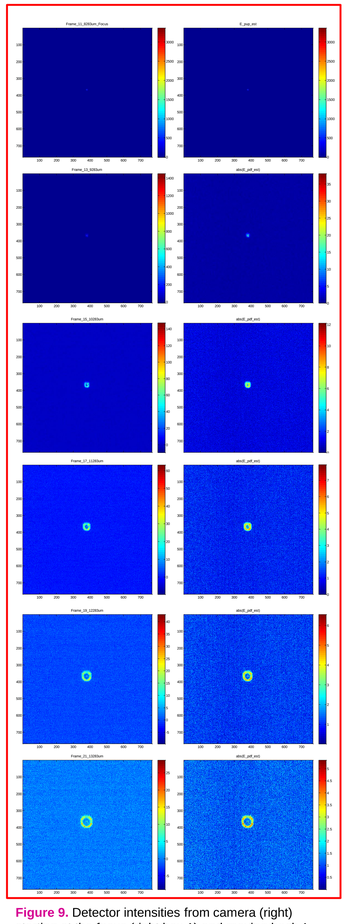

Figure 9. Detector intensities from camera (right) starting at the focus (right box 1) and moving back 1 mm per step. Mathematical manipulation (left) of focus intensity to generate images in 1 mm increments away from the focus.

RESULTS

Explanation of Misell Algorithm

The Misell Algorithm (Figure 3) begins with a Gaussian beam profile created on a pupil (Figure 1) shown in box 1. This profile is then subjected to wavefront error using high order Zernike polynomials. Box 2 shows the absolute value of this wavefront error returns to the original beam. Box 3 shows the complex components of the wavefront error. The Fourier transform of the pupil is taken, and the complex components are displayed in box 4. Boxes 1-4 serve as an expected wavefront error that could be seen in the testbed. Subsequent steps will estimate this error mathematically. Box 5 begins with the same original beam profile. Boxes 6 and 7 show the Fourier propagation of this beam 1 mm on both sides. The inverse Fourier transform is then taken of these images and the resulting images for 6 and 7 are shown in boxes 8 and 9 respectively. These images are then filtered using parameters shown in box 10. Box 11 is a cross-sectional view of box 10 showing the sharp drop in the filter. The final estimate of box 3 is then shown in box 12.

The Misell Algorithm (Figure 8) also begins with a Gaussian beam profile (box 1), but this beam more closely resembles the actual light of the SCDU testbed. This profile is then subjected to wavefront error using high order Zernike polynomials. Box 2 shows the absolute value of this wavefront error returns to the original beam. Box 3 then shows the complex components of the wavefront error. The Fourier transform of the pupil is taken, and the real components are displayed in box 4 while the complex components are shown in box 5. Now boxes 1-5 serve as the expected wavefront error possible in the testbed. Box 6 begins the estimates of the wavefront error starting with the same beam profile. Box 7 shows the Fourier propagation of this beam 0.4 mm in front of the pupil. The inverse Fourier transform is then taken of box 7 and displayed in box 8. This image is then filtered using parameters shown in box 9. Box 10 is a cross-sectional view of box 10 showing a much broader drop in the filter. The final estimate of box 3 is then shown with the complex components in box 11 and the absolute value shown in box 12.

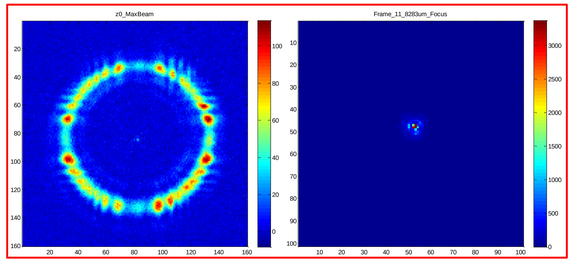

Figure 10. Intensity measurements of HeNe collimated beam at position closest to parabolic mirror (left) and position at focus (left).

Data Analysis

First Run: The focus was initially determined at a Oriel® position of 8283.3µm with a standard deviation of 20.0675µm. This position then became the target measurement. Intensity measurements were taken every 500µm to a maximum distance of 5000µm to each side of this focus. The intensity measurement for the focus was evaluated using a refined Misell algorithm (Figure 9). The focus intensity was Fourier transformed 500 µm behind the image. The amplitude of the intensity data at this recorded position was then multiplied by the imaginary exponential of this transform. This created image was then compared to the detector intensity recorded at that position (Figure 9).

Second Run: Before the second run the settings had to be realigned because the image was not centered on the detector camera. After realignment the new focus was found to be 8234.4µm with a standard deviation of 12.0237µm. This position became the new target measurement. Intensity measurements were taken every 500µm to a maximum distance of 6500µm to each side of the focus. The intensity measurement for the focus was evaluated using a refined Misell algorithm. The focus intensity was Fourier transformed 500 µm behind the image. The amplitude of the intensity data at this recorded position was then multiplied by the imaginary exponential of this transform. This created image was then compared to the detector intensity recorded at that position.

REFERENCES

1. "James C. Wyant - Zernike Equations." *College of Optical Sciences - The University of Arizona*. http://www.optics.arizona.edu/jcwyant/Zernikes/ZernikeEquations.htm.
2. R. Soumner, L. Pueyo, A. Sivaramakrishnan, R.J. Vanderbei; *Fast computation of Lyot-styl coronagraph propagation,* Optical Society of America 2008; arXiv:0711.0368v1.
3. M.L. Misell; *A method for the solution of the phase problem in electron microscopy,* J. Phys. D: Appl. Phys.,Vol. *6,* 1973.

ACKNOWLEDGEMENTS

We would like to thank NASA's KSGC (Kentucky Space Grant Consortium Program) for funding this research project.